DAM BREAK FLOW ANALYSIS WITH APPROXIMATE RIEMANN SOLVER

Dae-Hong Kim

Korea Institute of Water and Environment, Korea Water Resources Corporation, Daejeon, Korea

Abstract: A numerical model to analyze dam break flows has been developed based on approximate Riemann solver. The governing equations of the model are the nonlinear shallow-water equations. The governing equations are discretized explicitly by using finite volume method and the numerical flux are reconstructed with weighted averaged flux (WAF) method. The developed model is verified. The first verification problem is about idealized dam break flow on wet and dry beds. The second problem is about experimental data of dam break flow. From the results of the verifications, very good agreements have been observed

1. INTRODUCTION

The flows by dam break would change abruptly in space and time on large area. These flows can be simulated by two-dimensional hyperbolic type shallow-water equations.

Many numerical models which analyze dam break flows have been developed. Glaister (1988) used a finite difference method based on a flux difference splitting to solve the one-dimensional dam break problem. Mingham and Causon (1999) described a finite volume method to simulate two-dimensional shallow-water flow. They used a monotone upstream-centered scheme for conservation law (MUSCL) reconstruction and Riemann solver. Fujihara et al. (2000) presented a second-order accurate Godunov type finite volume numerical model for the two-dimensional conservative hyperbolic shallow-water equations on

a nonorthogonal curvilinear coordinate. Zhao et al. (1994, 1996) developed a finite volume model with first-order accuracy on an unstructured gird system. Wang et al. (2000) employed a total variation diminishing (TVD) finite difference scheme and Kim et al. (2002) employed a TVD finite volume scheme to solve dam break problems. All of these models produced very good results but they were applied to only flat bottoms.

Fraccarollo and Toro (1995) and Brocchini et al. (2001) proposed second-order accurate numerical schemes of the Godunov type for two-dimensional problems on wet and dry beds. On the basis of the shock capturing weighted averaged flux scheme, two-dimensional flows were solved by sequences of argumented one-dimensional flows in the numerical model. Zoppou and Stephen (1999, 2000) used a frac-

tional step method and first-order approximate Riemann solver based on the WAF method to solve shallow-water equations on an unstructured triangular grid. They obtained a second-order accuracy in the Cartesian grid. Bradford and Sanders (2002) proposed a finite volume method coupled with MUSCL data reconstruction and Riemann solver. These models were considered to resolve shock very accurately and give good results on uneven topography.

Because the dam break flows have very complicate physical characteristics, in order to analyze the flows it is necessary to integrate all properties developed in numerical models which are mentioned above. That is, the numerical model which has an ability to capture shocks, handle a complex geometry, and simulate flows on wet and dry beds simultaneously can be applied dam break flows. In our review, only Fraccarollo and Toro's (1995) and Zoppou and Stephen's (1999, 2000) models can be applied to practical dam break problems.

In the present study, the development process of a numerical model which can be used to analyze various dam break flows is presented. Also, some flux limiters to control the numerical oscillations related with second-order accurate scheme are tested and in order to verify the accuracy and ability of the numerical model, some test problems are solved.

2. GOVERNING EQUATIONS AND NUMERICAL SCHEME

2.1 Governing equations

The nonlinear shallow-water equations in conservative form including bottom slopes are adequate to describe the flow motions by dam break are shown as follows:

$$\frac{\partial \mathbf{U}}{\partial t} + \frac{\partial \mathbf{E}}{\partial x} + \frac{\partial \mathbf{F}}{\partial y} = \mathbf{S} \tag{1}$$

In equation (1), the vector of conserved variables $\mathbf{U}$, the flux vectors $\mathbf{E}$ and $\mathbf{F}$ in the x - and y-directions and the source term $\mathbf{S}$ can be written as

$$\mathbf{U} = \begin{bmatrix} h \\ hu \\ hv \end{bmatrix}, \quad \mathbf{E} = \begin{bmatrix} hu \\ hu^2 + \frac{1}{2}gh^2 \\ huv \end{bmatrix},$$

$$\mathbf{F} = \begin{bmatrix} hv \\ huv \\ hv^2 + \frac{1}{2}gh^2 \end{bmatrix}, \quad \mathbf{S} = \begin{bmatrix} 0 \\ gh(S_{ox} - S_{fx}) \\ gh(S_{oy} - S_{fy}) \end{bmatrix} \tag{2}$$

where h is the total water depth, u and v are the velocities in the x- and y-directions, g is the acceleration due to gravity, and S_{ox} and S_{oy} are bed slope components in the x- and y-directions, respectively. S_{fx} and S_{fy} are bottom friction terms in the x- and y-directions, respectively.

By integrating the shallow-water equations (1) over an arbitrary cell, the equations of the finite volume method can be obtained as

$$\frac{\partial}{\partial t} \int_A \mathbf{U} dA + \oint_\Omega \mathbf{G} \cdot \mathbf{n} d\Omega = \oint_\Omega \mathbf{S} d\Omega \tag{3}$$

where $\mathbf{G}$ is the flux tensor, A and Ω are the surface area and boundary of the control volume L, respectively, and $\mathbf{n}$ is the outward unit vector normal to the boundary. By introducing rotational invariance the equation (3) becomes

$$\frac{d\mathbf{U}}{dt} + \frac{1}{|A|} \sum_{s=1}^N \int_{A_s}^{A_{s+1}} \mathbf{T}_s^{-1} \mathbf{G}(\mathbf{T}_s \mathbf{U}) dA = \mathbf{S} \tag{4}$$

where $\mathbf{T}_s$ is the transformation matrix and by using equation (4), two-dimensional problems can be applied on unstructured grids. More de-

tailed descriptions on governing equations and unstructured grid system can be found in Kim et al. (2002), hence those are not repeated here again.

2.2 HLLC approximate Riemann solver

Billett, et al. (1997) used the HLLC approximate Riemann solver to solve the one-, two- and three-dimensional hyperbolic problems and Kim et al. (2002) applied it on analysis of shallow water problems. The details of HLLC approximate Riemann solver are written on those materials and then this paper has only brief descriptions.

For the convenience, if we assume that the flow varies only x-direction and neglect the source terms then the equation (1) becomes

$$\frac{\partial U}{\partial t} + \frac{\partial E}{\partial x} = 0 \tag{5}$$

In equation (5), U is a vector of three conserved variables. Therefore the system of equation (5) which is hyperbolic has three distinct real eigen values and the solution to Riemann problem consists of three waves with speeds S

separating four constant states as described in Figure 1. Therefore, as shown in Figure 1, in HLLC approximate Riemann solver, the variables are separated as

$$\tilde{U}(x,y) = \begin{cases} U_L & \text{for } 0 \le S_L \\ U_L^* & \text{for } S_L \le 0 \le S_* \\ U_R^* & \text{for } S_* \le 0 \le S_R \\ U_R & \text{for } S_R \le 0 \end{cases} \tag{6}$$

and the reconstructed numerical flux can be written as

$$E_{i+1/2}^{HLLC} = \begin{cases} E_L & \text{for} \\ E_L^* = E_L + S_L(U_L^* - U_L) & \text{for} \\ E_R^* = E_R + S_R(U_R - U_R^*) & \text{for} \\ E_R & \text{for} \end{cases}$$

$$0 \le S_L$$
$$S_L \le 0 \le S_* \tag{7}$$
$$S_* \le 0 \le S_R$$
$$S_R \le 0$$

where the subscript $i+1/2$ means an intercell boundary, L and R mean the left and right computational cells. The wave speeds are given as
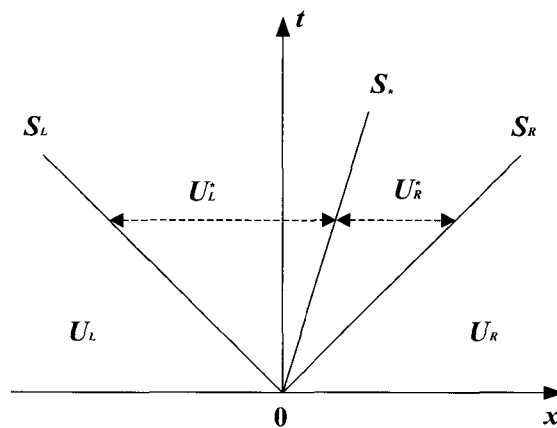

Figure 1. HLLC approximate Riemann solver structure

$$S_L = \min(u_L - \sqrt{gh_L}, \ u_* - \sqrt{gh_*})$$

$$S_* = u_* = \frac{u_L + u_R}{2} + \sqrt{gh_L} - \sqrt{gh_R} \qquad (8)$$

$$S_R = \max(u_R + \sqrt{gh_R}, \ u_* + \sqrt{gh_*})$$

where h_* is given as

$$h_* = \frac{(u_L + 2\sqrt{h_L} - u_R - 2\sqrt{h_R})^2}{16} \qquad (9)$$

An advantage of HLLC approximate Riemann solver is that it uses wave speeds based on analytic dry front speeds, consequently, it produces better results than Roe's solver on dry bed.

That is, equation (8) is valid only when there exists a finite water depth in the entire computational domain. However, if a dry bed exists then no shock exists and wave speeds should be used by another analytic method. In HLLC scheme, the wave speed of left side dry case ($h_L=0$ and $h_R>0$) and right side dry case ($h_R>0$ and $h_L>0$) are given as

$$\begin{array}{ll} S_L = u_R - 2\sqrt{gh_R} & S_L = u_L - \sqrt{gh_L} \\ S_* = S_L & \text{and} \quad S_* = S_R \\ S_R = u_R + \sqrt{gh_R} & S_R = u_L + 2\sqrt{gh_L} \end{array} \qquad (10)$$

In order to control the numerical oscillations related with second-order accuracy TVD scheme is employed. The numerical flux at intercell boundary including flux limiter is given as

$$\mathbf{E}_{i+1/2} = \frac{1}{2}(\mathbf{E}_i + \mathbf{E}_{i+1}) - \frac{1}{2}\sum_{k=1}^{N} sign(c_k)\varphi^k_{i+1/2}\Delta\mathbf{E}^k_{i+1/2} \qquad (11)$$

in which $\mathbf{E}^k_{i+1/2} = \mathbf{E}(\mathbf{U}^k_{i+1/2})$, c_k is the Courant number for a wave k of speed S_k and $\Delta\mathbf{E}^k_{i+1/2} = \mathbf{E}^{k+1}_{i+1/2} - \mathbf{E}^k_{i+1/2}$. $\varphi^k_{i+1/2}$ is a flux limiter function related TVD scheme, which controls

the numerical oscillations. Four flux limiter functions, that is SUPERA, VANLEE, VANALB and MINAAA written on Toro (1999), are used and compared with each other in later section. The limiters used in this study are given as

$$\varphi_{SUPERA}(r,k) = \begin{cases} 1 & \text{for} & r \le 0 \\ 1-2(1-|c_k|)r & \text{for} & 0 \le r \le 1/2 \\ |c_k| & \text{for} & 1/2 \le r \le 1 \\ 1-(1-|c_k|)r & \text{for} & 1 \le r \le 2 \\ 2|c_k|-1 & \text{for} & 2 \le r \end{cases} \qquad (12)$$

$$\varphi_{VANLEE}(r,k) = \begin{cases} 1 & \text{for} & r \le 0 \\ 1-\dfrac{(1-|c_k|)2r}{1+r} & \text{for} & r \ge 0 \end{cases} \qquad (13)$$

$$\varphi_{VANALB}(r,k) = \begin{cases} 1 & \text{for} & r \le 0 \\ 1-\dfrac{(1-|c_k|)r(1+r)}{1+r^2} & \text{for} & r \ge 0 \end{cases} \qquad (14)$$

$$\varphi_{MINAAA}(r,k) = \begin{cases} 1 & \text{for} & r \le 0 \\ 1-(1-|c_k|)r & \text{for} & 0 \le r \le 1 \\ |c| & \text{for} & r \ge 1 \end{cases} \qquad (15)$$

2.3 Source Term Treatment

The equation (5) does not contain the source terms. The form of equation (5) involving source terms can be solved by the splitting technique. That is, for the x-direction

$$\begin{array}{l} PDE : \dfrac{\partial \mathbf{U}}{\partial t} + \dfrac{\partial \mathbf{E}}{\partial x} = 0 \\ IC \ : \mathbf{U}^k \end{array} \Biggr\} \xrightarrow{\Delta t} \mathbf{U}^{k+1}_* \quad ,$$

$$\begin{array}{l} ODE : \dfrac{d\mathbf{U}}{dt} = \mathbf{S}_x \\ IC \ : \mathbf{U}^{k+1}_* \end{array} \Biggr\} \xrightarrow{\Delta t} \mathbf{U}^{k+1} \qquad (16)$$

The procedure for analysis of flux part is

written above paragraph. The source part can be solved by ordinary differential solver. In this study the source terms are discretized by using pointwise scheme and solved by explicit Euler method. More details about theoretical aspects of splitting technique a governing equation into flux and source part and ordinary differential solver are explained well in Zoppou and Stephen (1999, 2000) and Hu et al. (2000).

By using a fractional step method, the two-dimensional shallow-water equations can be split into two augmented one-dimensional equations along x- and y-directions. The solutions of each fractioned equation can be obtained by the numerical technique described on above paragraph. If we denote $x^{\Delta t}$ as the procedure of equations (16) and denote $y^{\Delta t}$ for y-direction, respectively, then the approximate solution of two-dimensional problem can be obtained by using the equation (17) which is second-order accurate in space.

$$\mathbf{U}^{k+1} = y^{\Delta t/2} x^{\Delta t/2} y^{\Delta t/2} x^{\Delta t/2} (\mathbf{U}^k) \qquad (17)$$

2.4 Boundary conditions

Representatively, two types of boundary conditions are modeled. The reflective boundary condition is given as

$$\mathbf{U}_b = \begin{pmatrix} h_{b-1} \\ -u_{b-1} \\ v_{b-1} \end{pmatrix}, \quad \mathbf{U}_{b+1} = \begin{pmatrix} h_{b-2} \\ -u_{b-2} \\ v_{b-2} \end{pmatrix} \qquad (18)$$

and the transmissive boundary condition is given as

$$\mathbf{U}_b = \mathbf{U}_{b-1}, \quad \mathbf{U}_{b+1} = \mathbf{U}_{b-2} \qquad (19)$$

where $\mathbf{U}_b$ means a conservative variable vector at right end boundary in split one- dimensional

equations.

3. VERIFICATION OF NUMERICAL MODEL

In order to verify the capability of numerical model based on HLLC approximate Riemann solver, comparisons are made with analytic solutions and experimental data.

3.1 Verifications with Analytic solutions of Idealized Dam Break Flows

To verify the accuracy of the developed model, dam break flows on horizontal bottom are simulated and compared with analytical solutions (Toro, 2001). The channel length is 100 m and the dam located on center of the channel.

The Figures 2(a)~(f) describe the water surface obtained at 8.0 second after dam break. In these applications, a finite water depth existed all over the computational domain, that is, upstream water depth is 1.0 m and the downstream water depth is 0.1 m. All of the computed results show reasonable. In Figure 2(a), however, there is numerical diffusion originated from first- order accuracy upwind scheme and in Figure 2(b), there is numerical oscillation originated from second-order accuracy numerical scheme. Consequently, some discrepancies are shown around bore in Figures 2(a) and 2(b). The results shown in Figures 2(c)~(f) are obtained with four different flux limiters and seem to be very accurate.

The Figures 3 show the details of Figures 2. The discrepancies between the analytic solution and the computed result by second-order oscillatory scheme is largest and the computed result by first-order upwind scheme is following. Although the computed result with SUPERA flux limiter is most accurate among all computed results with flux limiters, the discrepancies are
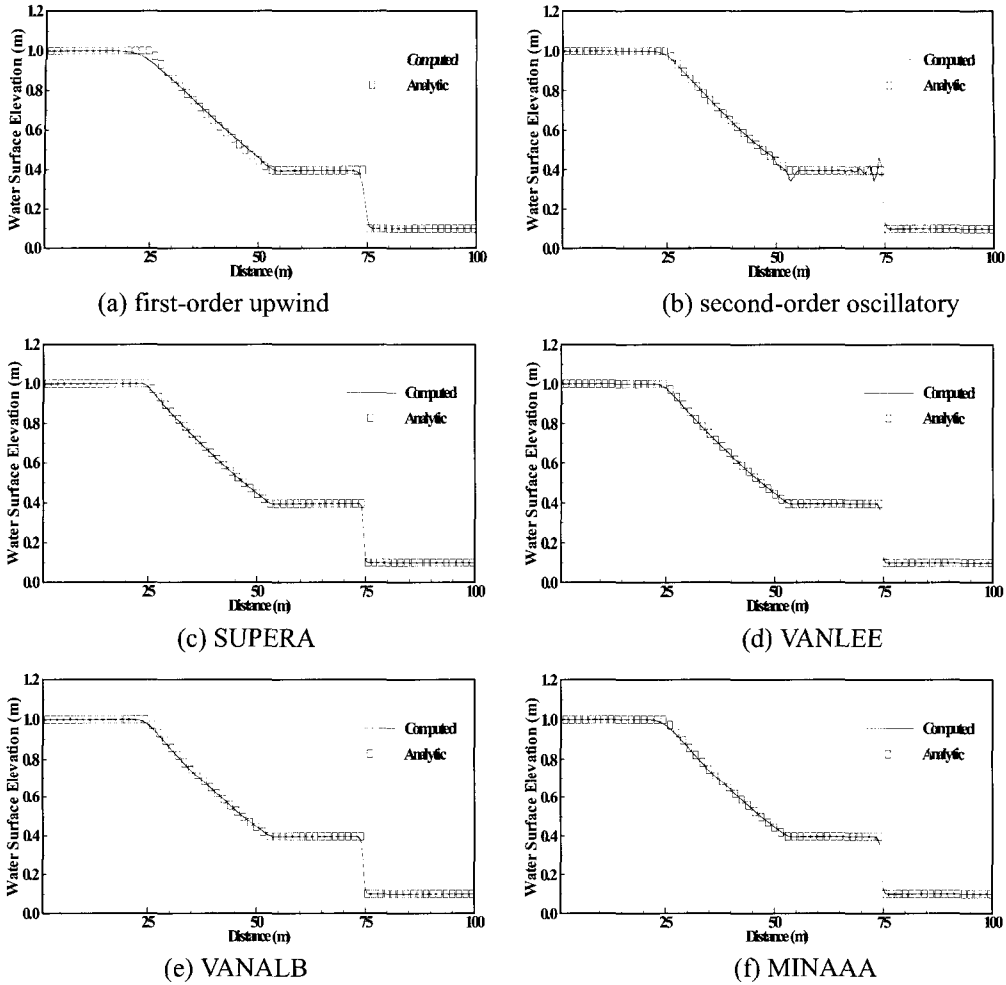
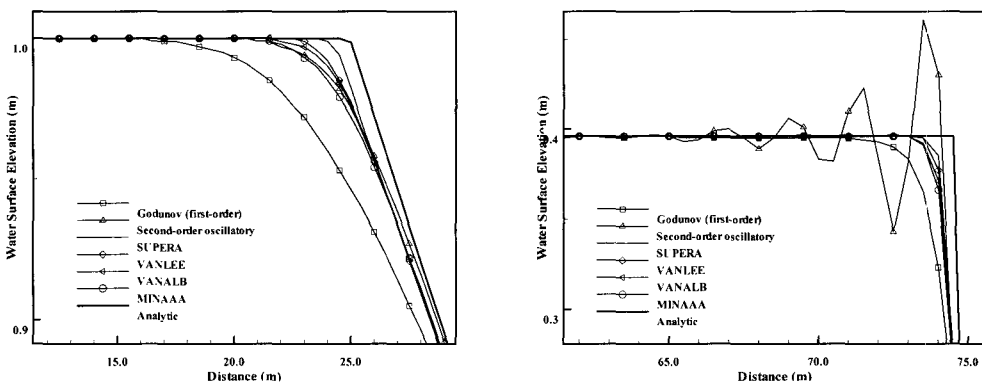Figure 2. Comparisons of analytic solutions and computed results with various flux limiters (wet bed)

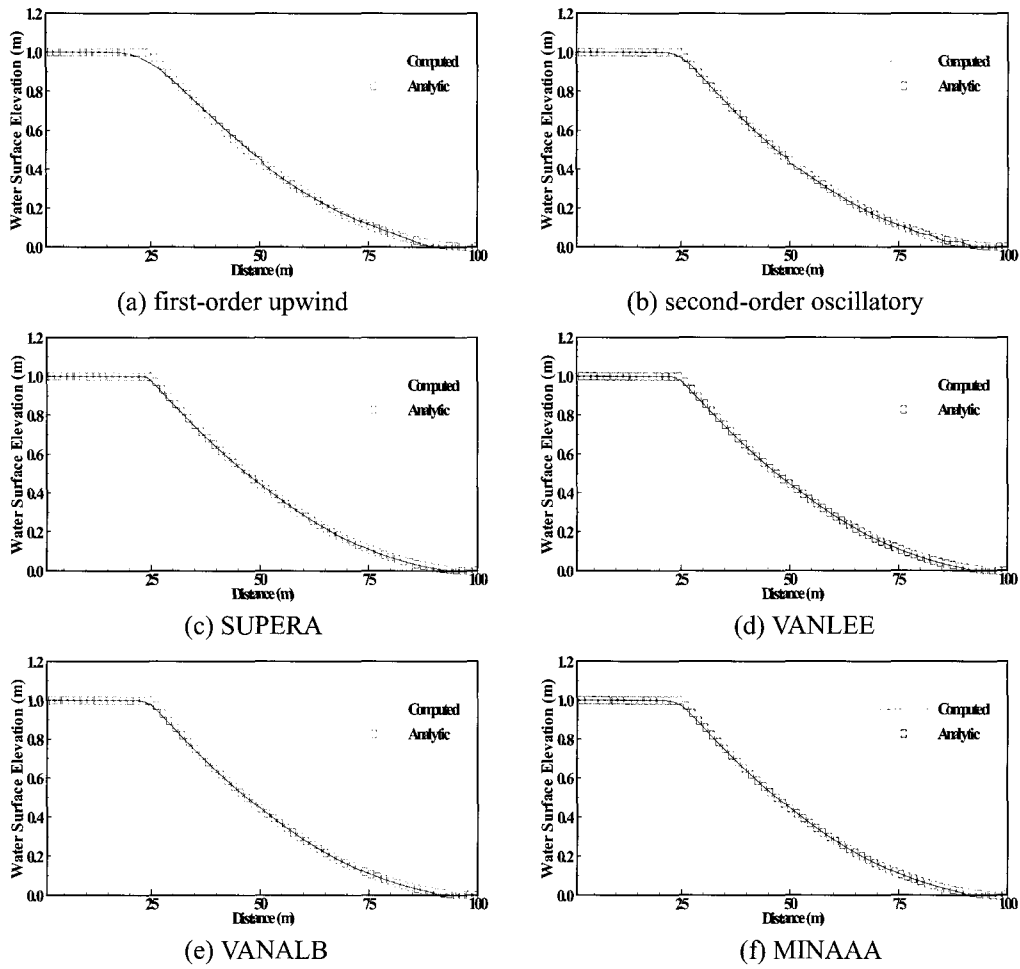Figure 3. Detail views of comparisons of analytic solutions and computed results (wet bed)

(a) first-order upwind

(b) second-order oscillatory

(c) SUPERA

(d) VANLEE

(e) VANALB

(f) MINAAA

Figure 4.   Comparisons of analytic solutions and cmputed results with various flux limiters (dry bed)
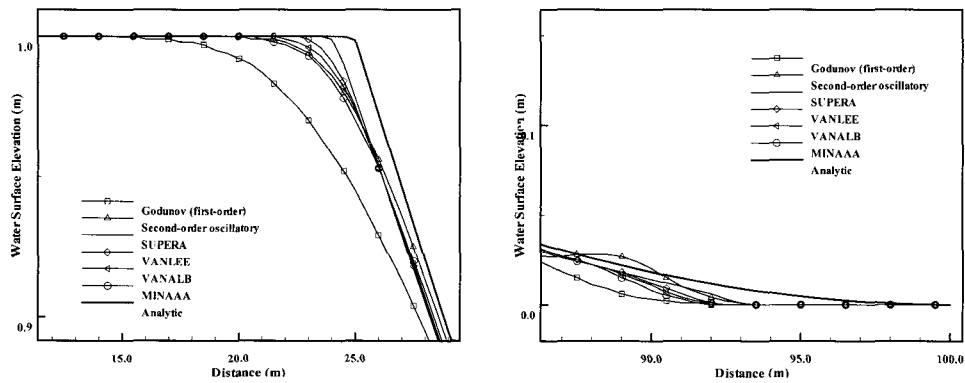

Figure 5. Detail views of comparisons of analytic solutions and computed results (dry bed)

very small and negligible.

The Figures 4(a)~(f) describe the water surface obtained at 8.0 second after dam break. In this case, a finite water depth existed only on upstream. On downstream, dry bed condition is applied, that is, upstream water depth is 1.0 m and the downstream water depth is 0.0 m. All of the computed results seem to be also reasonable. In Figure 4(a) and Figure 4(b), numerical diffusion originated from first-order accuracy upwind scheme and numerical oscillation originated from second-order accuracy numerical scheme are also shown like wet bed case. Consequently, some discrepancies are detected around bore in Figures 4(a) and 4(b). The results shown in Figures 4(c)~(f) obtained with four flux limiters and seem to be very accurate. Above mentioned, the developed model calculates the conserved variables with analytic method. Therefore the computed results around the boundaries between wet and dry beds are very accurate. The small difference mainly comes from that the computational hydraulic problems are solved on discretized domains. On discretized domains, the computed water depth is averaged depth by the area of each cell, which makes the computed water depth small.

The Figures 5 show the details of Figures 4. Similar to the wet bed case, the discrepancy between the analytic solution and the computed result by second-order oscillatory scheme is largest and the computed result by first-order upwind scheme follows. The computed result with SUPERA flux limiter is most accurate but the discrepancies between computed result by SUPERA and other flux limiters are very small and negligible, too.

3.2 Verification with Experimental Data

In the second verification, the numerical solutions are compared with experimental data. Bellos et al. (1992) investigated experimentally the flow depth in a converging-diverging open channel. Because of converging-diverging shape, slope and friction, it is impossible to obtain solutions by analytic methods.

The plan view of the channel is shown in Figure 6. As described on Figure 6, the channel length is 21.2m, the slope is 0.002, and the width varies from 0.6 m to 1.4 m. At the downstream end, free overfall conditions were applied and vertical walls were installed at the other sides. A dam is located on 8.5 m from upstream.

The upstream water surface elevation was 3.0 m and the downstream water depth was 0.0m, that is, dry bed condition was setup. During the numerical simulations, the Manning's roughness coefficient n is input by 0.013, the wall frictions were neglected, and SUPERA flux limiter was used.

The Figures 7(a)~(d) show the computed water surface elevation. In Figure 7(b) and 7(c), the water column depicted in Figure 7(a) is collapsed and the water surface elevation of upstream side descends down. On downstream side, the released water from upstream reservoir flow toward downstream end and overfall. Finally, almost of water was released 60 second after dam break as shown in Figure 7(d).

The Figures 8(a)~8(d) show the measured results and computed results on four points. The main reason of small discrepancy is caused by the frictionless wall conditions, use of Manning's equation that is derived from steady flow. Additionally, because we regard the flows in three-dimensional space as flows in two- dimensional space, it is natural that there are differences the computed results and measured data. In practical view, the computed results and the
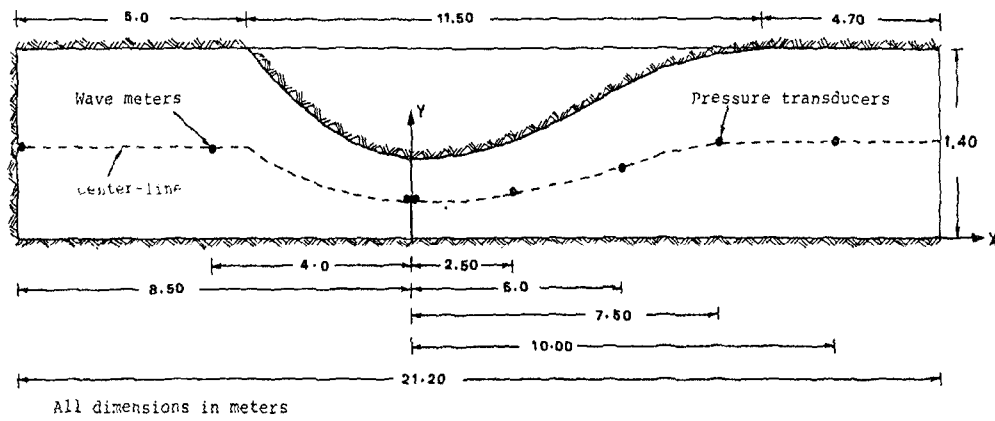
Figure 6. Schematic diagram of dam break flow experiment channel (Bellos et al. 1992)
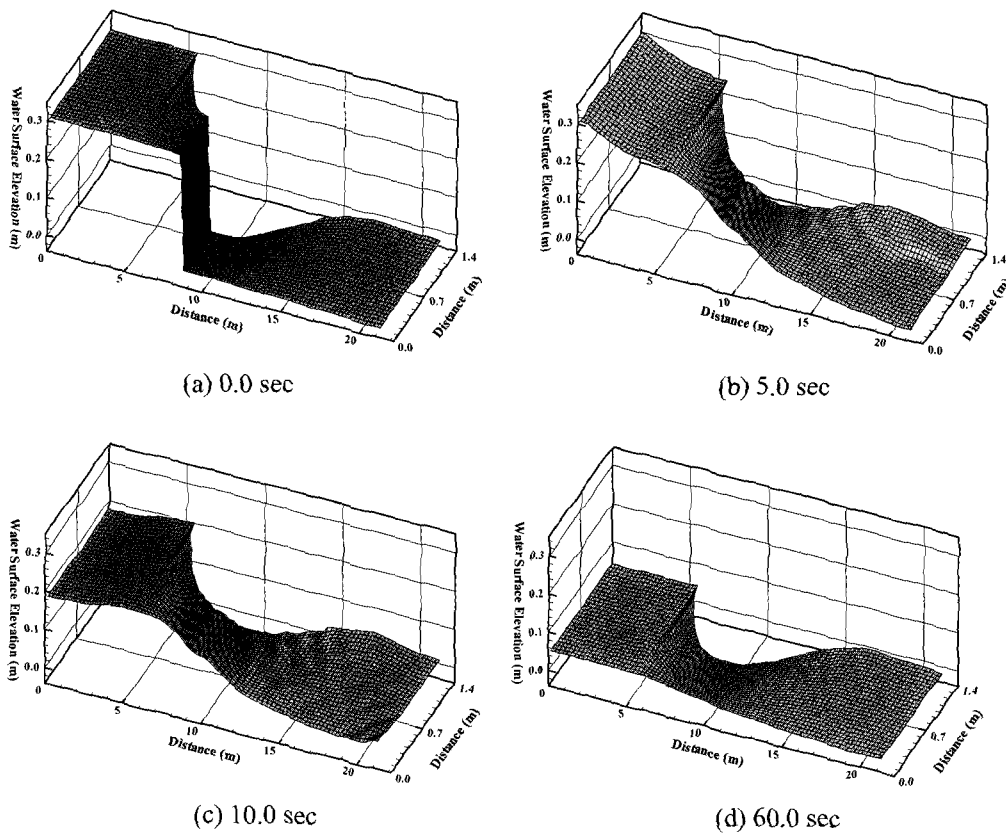

(a) 0.0 sec

(b) 5.0 sec

(c) 10.0 sec

(d) 60.0 sec

Figure 7. Snap shots of computed water surface elevation

(a) 8.5 m upstream from dam

(b) 4.0 m upstream from dam

(c) Upstream dam face

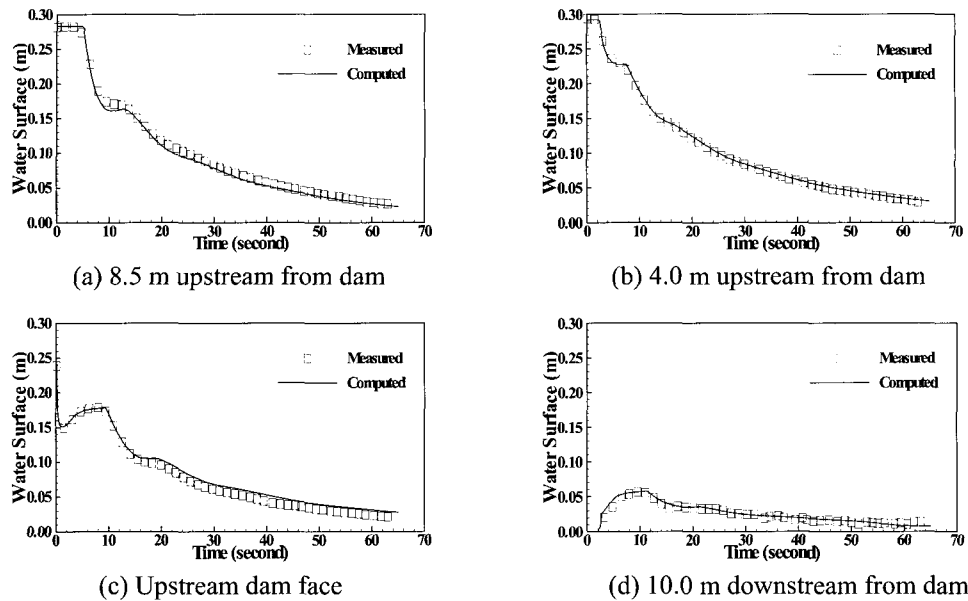(d) 10.0 m downstream from dam

Figure 8. Comparisons of measured data and computed results

measured data agree well and it can be concluded that the present model can be reliably applied on two-dimensional dam break flow predictions.

4. CONCLUSIONS

In the present study, a numerical model to analyze the two-dimensional dam break flows based on HLLC approximate Riemann solver is developed and verified. The advantage of approximate Riemann solver is to capture the shock generated with dam break. The numerical oscillations commonly observed in second-order accuracy are controlled by exploiting four flux limiters.

In order to verify the accuracy and applicability of the presented model, idealized dam break flow problems on wet and dry beds are tested. Obtained computed results are compared with available analytic solutions and measured data. The computed results with flux limiters are

more accurate than the computed results without flux limiter. The SUPERA limiter gives the most accurate results but the discrepancies are negligible. The computed results from the simulations for experiment by Bellos et al. also show very good results. Consequently, the numerical model and numerical techniques are very robust to analyze and to simulate dam break flows.

REFERENCES

Bellos, C. V., Soulis, J. V., and Sakkas, J. G. (1992). "Experimental investigation of two-dimensional dam-break induced flows. " *Journal of Hydraulic Research*, 30(1), 47-63.

Billett, S. J., and Toro, E. F. (1997). "On WAF-Type Schemes for Multidimensional Hyperbolic Conservation Laws. " *Journal of Computational Physics*, 130(1), 1-24.

Bradford, S.F., and Sanders, B.F. (2002). "Finite-volume model for shallow-water

flooding of arbitrary topography. " *Journal of Hydraulic Engineering*, ASCE, 128(3), 289-298.

Brocchini, M., Bernetti, R., Mancinelli, A., and Albertini, G. (2001). "An efficient solver for nearshore flows based on the WAF method." *Coastal Engineering*, 43, 105-129.

Glaister, P. (1988). "Approximate Riemann solutions of the shallow water equations." *Journal of Hydraulic Research*, 26(3), 293-306.

Hu, K., Migham, C.G., and Causon, D.M. (2000). "Numerical simulation of wave overtopping of coastal structures using the non-linear shallow water equations." *Coastal Engineering*, 41, 433-465.

Kim, D. H., Kim, W. G., Chae, H. S. and Park, S. G. (2002). "Development of 2D Dam Break Flow Analysis Model using Fractional Step Method. " *Water Engineering Research*, 3(1), 23-30.

Mingham, C.G., and Causon, D.M. (1999). "Calculation of unsteady bore diffraction using a high resolution finite volume method." *Journal of Hydraulic Research*, 38(1), 49-56.

Fraccarollo, L., and Toro, E.F. (1995). "Experimental and numerical assessment of the shallow water model for two-dimensional dam-break type problems." *Journal of Hydraulic Research*, 33(6), 843-864.

Fujihara, M., and Borthwick, G.L. (2000). "Godunov-type solution of curvilinear shallow-water equations." *Journal of Hy-*

draulic Engineering, ASCE, 126(11), 827-836.

Toro, E.F. (1999). *Riemann solvers and numerical methods for fluid dynamics*, Springer.

Toro, E.F. (2001). *Shock-capturing methods for free-surface shallow flows*. John Wiley & Sons, Ltd.

Wang, J.S., Ni, H.G., and He, Y.S. (2000). "Finite-difference TVD scheme for Computation of dam-break problems." *Journal of Hydraulic Engineering*, ASCE, 126(4), 253-262.

Zhao, D.H., Shen, H.W., Lai, J.S., and Tabios III, G.T. (1996). "Approximate Riemann solvers in FVM for 2d hydraulic shock wave modeling." *Journal of Hydraulic Engineering*, ASCE, 122(12), 692-702.

Zhao, D.H., Shen, H.W., Tabios III, G.Q., Lai, J.S., and Tan, W.Y. (1994). "A finite volume two-dimensional unsteady flow model for river basins." *Journal of Hydraulic Engineering*, ASCE, 120(7), 863-883.

Zoppou, C., and Stephen, R. (1999). "Catastrophic collapse of water supply reservoirs in urban areas." *Journal of Hydraulic Engineering*, ASCE, 125(7), 686-695.

Zoppou, C., and Stephen, R. (2000). "Numerical solution of two-dimensional unsteady dam break." *Applied Mathematical Modelling*, 24, 457-475.

Korea Institute of Water and Environment, Korea Water Resources Corporation, Daejeon, Korea

(E-mail : iceman@kowaco.or.kr)